Confinement-Induced Clustering of H2 and CO2 Gas Molecules in Hydrated Nanopores

Journal:	*Physical Chemistry Chemical Physics*
Manuscript ID	CP-COM-12-2023-006024.R1
Article Type:	Communication
Date Submitted by the Author:	05-Feb-2024
Complete List of Authors:	Choudhary, Aditya; Sandia National Laboratories Ho, Tuan; Sandia National Laboratories, Geochemistry

Confinement-Induced Clustering of H_2 and CO_2 Gas Molecules in Hydrated Nanopores

Aditya Choudhary and Tuan A. Ho*

Geochemistry Department, Sandia National Laboratories, Albuquerque, NM 87185, USA

**Corresponding author:* *taho@sandia.gov*

Abstract

Gas molecule clustering within nanopores holds significance in the field of nanofluidic, biology, gas adsorption/desorption, and geological gas storage. However, the intricate roles of nanoconfinement and surface chemistry that govern the formation of gas clusters remain inadequately explored. In this study, through free energy calculation in molecular simulations, we systematically compared the tendencies of H_2 and CO_2 molecules to aggregate within hydrated hydrophobic pyrophyllite and hydrophilic gibbsite nanopores. The results indicate that nanoconfinement enhances gas dimer formation in nanopores, irrespective of surface chemistry. However, surface hydrophilicity prohibits the formation of gas clusters larger than dimers, while large gas clusters form easily in hydrophobic nanopores. Despite H_2 and CO_2 both being non-polar, larger quadrupole moment of CO_2 leads to a stronger preference for dimer/cluster formation compared to H_2. Our results also indicate that gas prefers to enter the nanopore as individual molecule but exits the nanopores as dimers/clusters. This investigation provides a mechanistic understanding of gas cluster formation within nanopores that are relevant to various applications, including geological gas storage.

1. Introduction

The clustering of gas molecules to form nanoscale bubbles in a liquid or gas phase has widespread application in nanofluidics,[1] water treatment,[2] gas adsorption/desorption,[3] geological gas storage,[4] mineral recovery,[5] ultrasound imaging, and drug delivery.[6] In nanofluidics, nanobubbles can plug nanochannels and divert electrolyte flows through interfacial electrolyte film,[1] thereby controlling the ionic conductance through nanopores.[7] In general, nanobubbles can impede,[7] gate,[8] enhance,[8] and drive selective mass transport through nanopores, which hold immense significance in biological systems. Near the surface of the confined region, nanobubbles can exist as spherical-cap-shaped bubbles, a pancake-like gas layer,[9] or a flat gas layer that covers the entire surface,[10] as observed using atomic force microscopy (AFM).[10, 11] A flat gas layer near a surface affects the flow of water or the movement of solutes through water[12] by changing the boundary condition[13] and altering long-range attractive forces between hydrophobic surfaces immersed in solutions.[14] The formation of nanobubbles on surfaces strongly depends on surface hydrophobicity, the commensuration of the spatial dimensions of the hydrophobic domains, and the equilibrium topology of nanobubbles.[15]

In CO_2 geological sequestration, the clustering of CO_2 within hydrated clay interlayers enhances the amount of CO_2 trapped inside Earth's nanoporous materials but can dehydrate nanopores, potentially creating a pathway for transport and leakage in gas storage systems such as CO_2 sequestration, CH_4 and H_2 storage.[16] In nanoporous materials like a metal-organic frameworks,[3] gas clustering controls gas desorption. When confined gas molecules have strong gas-gas intermolecular interaction, desorption proceeds via an unexpected metastable state, where gas molecules form clusters within the nanopores, temporarily decelerating the desorption rate.[3] This leads to a rate of desorption many orders of magnitude slower than that of adsorption.[17] The diffusion of gas molecules is governed by the dynamics of molecular clusters, whether they are stable or metastable, where the energy barriers for fragmentation of molecular clusters are considerably higher than monomer diffusion barriers.[18]

The coexistence of gas bubbles/clusters and liquid in nanopores is due to: (i) the presence of gases in a nanopore before the intrusion of liquid, (ii) the injection of gases into a liquid-filled nanopore, and (iii) the equilibrium of gases within a nanopore with the gases outside the nanopores. In the last case, the solubility of gas in the liquid phase is critical. Numerous studies have demonstrated that nanoconfined water enhances the solubility of gas molecules compared to bulk water, a phenomenon known as gas over-solubility.[19-21] Gas over-solubility in nanopores occurs either because gas molecules adsorb at the liquid/solid interface or because gas molecules occupy regions of low liquid density formed by the layering of solvent molecules under confinement.[22, 23] This phenomenon in triphasic systems has significant applications in the fields of catalysis,[24, 25] CO_2 storage,[4] and oil recovery.[26]

Despite the growing interest in the formation of gas nanobubbles/clusters within confined environments, no systematic study has been conducted to reveal the nanoconfinement effect on gas cluster formation, especially in sub-nanometer nanopores. When nonpolar gases are confined in hydrated nanopores, gas clustering can be related to the hydrophobic effect/interaction.[27] Consequently, the central questions addressed in this work revolve around how nanoconfinement and surface chemistry modify these interactions and how these altered interactions subsequently influence gas cluster formation. Given that nanoconfinement alters many physicochemical and thermodynamic properties of confined species compared to their characteristics in a bulk state,[28-36] it is reasonable to assume that nanoconfinement significantly enhances or suppresses these interactions, which ultimately reflect in clustering of gas molecules.

In this study, we employed molecular simulations with free energy calculations to achieve four main objectives: (i) Evaluate the nanoconfinement effect on gas clustering by comparing the free energy of gas dimer formation in bulk water with that in two-layer and one-layer of confined water; (ii) Examine the propensity of gas molecules to aggregate within hydrophobic and hydrophilic nanopores; (iii) Assess the aggregation tendency of H_2 and CO_2, which are non-polar in nature with significantly different polarizabilities (CO_2: 2.51×10^{-24} cm^3; H_2: 0.80×10^{-24} cm^3) and quadrupole moments (CO_2: $14.2 \times 10^{-40}\ \mathrm{C \cdot m^2}$; H_2: $1.7 \times 10^{-40}\ \mathrm{C \cdot m^2}$)[37] ; (iv) Investigate whether gas molecules prefer to enter a nanopore as a single molecule or as a gas dimer/cluster. The molecular insights presented in this study are crucial for advancing the fundamental understanding of gas molecule clustering within nanoconfined spaces.

2. Results and Discussion

We examine the tendency of two gas molecules to form a dimer, considered as the first step of gas cluster formation. We apply the well-tempered metadynamics[38] technique in molecular simulation to calculate the potential of mean force (PMF) as a function of distance *r* between two gas molecules in bulk water (Figure 1a), water confined in hydrophobic pyrophyllite (Figure 1b and c), and hydrophilic gibbsite (Figure 2a and b) nanopores. The pyrophyllite surface is hydrophobic because of the presence of siloxane (-Si-O-Si-) rings, whereas gibbsite surface is hydrophilic due to hydroxyl (-OH) groups (Supplementary Information (SI), Figure S1).[39] The size of the nanopore is tuned to accommodate two layers (2W) or one layer (1W) of water. All the molecular dynamics (MD) simulations are conducted using the LAMMPS package[40] at 300K and 1 atm, which is controlled through a Nosé–Hoover thermostat and barostat.[41, 42] The ClayFF[43] force field parameters are used for pyrophyllite and gibbsite, and SPC/E[44] for water. For CO_2 and H_2, we used TRaPPE[45] and 3-site models,[46] respectively. These force fields have shown consistent results with experiments.[47, 48] Because we used 3-site model for H_2 and CO_2, their interactions with other species including the surface are anisotropic. Indeed, H_2/H_2 interactions can be described well with an isotropic potential (e.g., a Lennard-Jones sphere). However, H_2/surface interaction can be anisotropic. Therefore, the use of 3-site model will capture H_2/surface anisotropic effect, if any. Also, nuclear quantum effect[49] is not considered in this work due to the use of classical force field. Including such effect could provide a more accurate description of interactions under confinement, which deserves a future study.[50, 51] See SI for more details about system setup and metadynamics simulation.

In bulk water, the PMF (i.e., the free energy) as a function of the distance r between the central atom of two CO_2 (Figure 1d, blue line) or H_2 (Figure 1e, blue line) decreases with increasing r, suggesting that two gas molecules prefer to stay as individual molecules. This can be explained by the probability $\mathrm{P_r}$ of finding one gas molecule from another gas molecule $\mathrm{P_r} = 4\pi r^2 \Delta \mathrm{r} g_r$, where $\mathrm{g_r}$ is the radial distribution function. The change in free energy is $\Delta\mathrm{G} = -\mathrm{k_B T ln P_r} = -\mathrm{k_B T}(\ln 4\pi\Delta\mathrm{r} g_r + 2\ln r)$ where $\mathrm{k_B}$ is the Boltzmann constant and T is the temperature. At a large r, the decrease in free energy is solely due to the entropic term $-2\mathrm{k_B T ln r}$ (*i.e.,* $\ln 4\pi\Delta\mathrm{r} g_r$ is constant). Note that the decrease in free energy is true only for a dilute condition, which is likely the case for gases with low solubility in water. A similar phenomenon is observed for the PMF of two gases in vacuum (Figure S4).

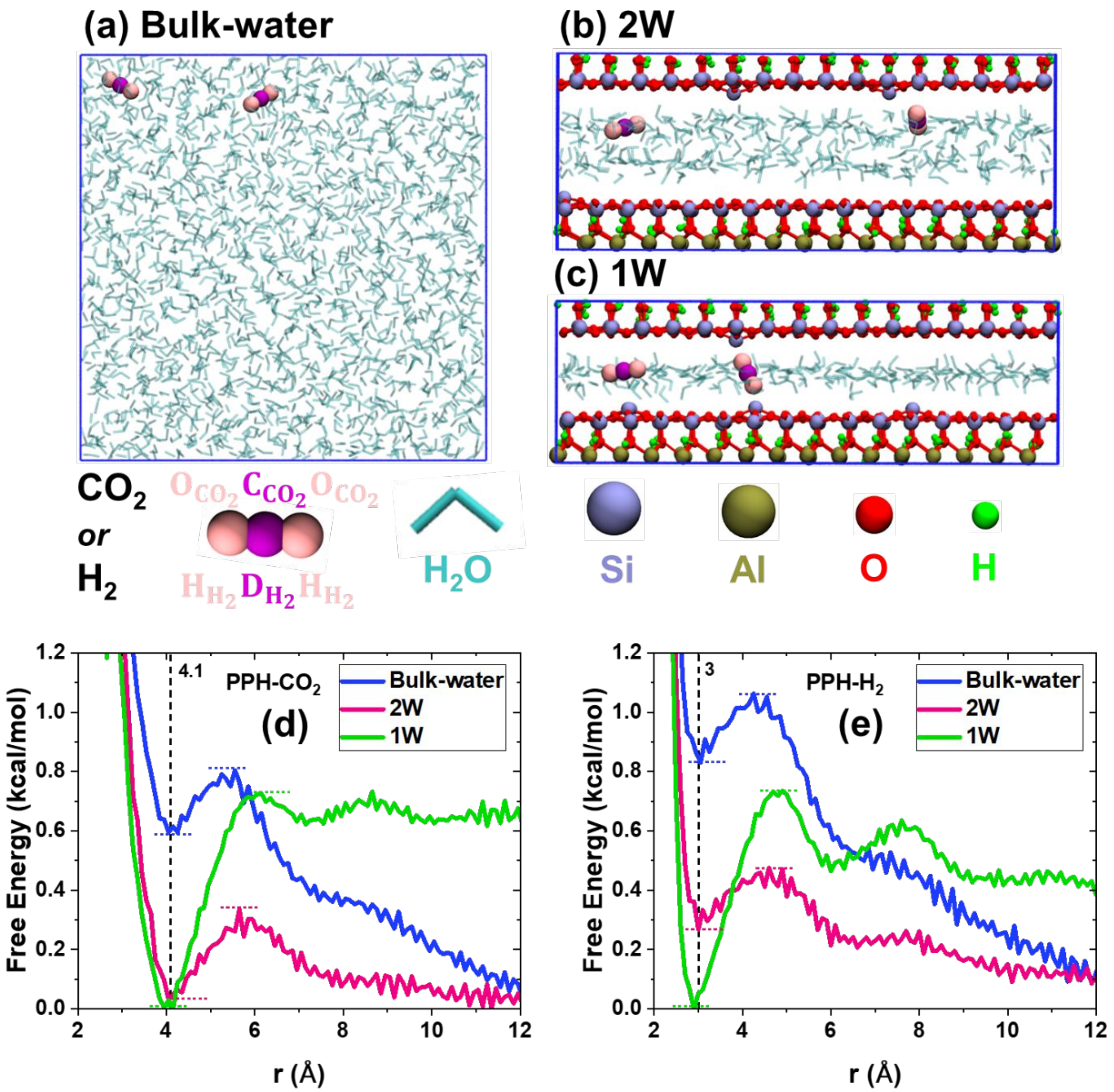

Figure 1. Typical snapshots of two CO_2 or H_2 molecules in (a) bulk water, (b) 2W, and (c) 1W pyrophyllite (PPH) interlayers. For pyrophyllite with 2W and 1W, the simulation box dimensions perpendicular to the surface are 16.26 Å and 13.26 Å, respectively. The color code for all atoms/molecules is provided under the figure. Note that D_{H_2}represents the center of mass of a H_2 molecule and the dummy atom of the H_2 model using in this work. The free energy profile as a function of distance r between two (d) CO_2 and (e) H_2 molecules in different environment. The convergence of the PMF calculation is reported in SI, Figure S2.

The PMF profile in bulk water also shows a local minimum, located at r equals 4.1 and 3 Å for CO_2 and H_2, respectively. At this minimum, two gas molecules form a dimer (no water molecules are between them). To separate two gas molecules from the dimer configuration, an activation energy barrier (ΔG^a) is required. The barrier is comparable for both gases, $\Delta G^a \sim 0.22$ kcal/mol. However, the driving force for such separation is stronger for H_2 ($\Delta G_{r = 3.0 \rightarrow 12Å} = -0.71$ kcal/mol) than for CO_2 ($\Delta G_{r = 4.1 \rightarrow 12Å} = -0.51$ kcal/mol). Note that we select 12Å to obtain a quantitative comparison of ΔG among different systems in this article. In other words, CO_2 is more likely to exist in a dimeric form than H_2 because of substantial quadrupole-quadrupole attraction.

Nanoconfinement significantly affects the free energy profiles of two gases. Yet, like bulk water, at larger distances, we observe a slight decrease in the free energy with increasing *r* for 2W and 1W pyrophyllite (magenta and green lines) systems. However, the decreasing trend reduces with an increase in nanoconfinement. Because unlike bulk systems, in two-dimensional (2D) systems like 2W and 1W, the probability P_r^{2D} of finding a gas molecule from another gas molecule is given by $P_r^{2D} = 2\pi r g_r \Delta r$ and the corresponding $\Delta G = -k_B T(\ln 2\pi \Delta r g_r + \ln r)$. At larger distances, the entropy term in 2D systems ($-k_B T \ln r$) is half that of bulk, resulting in only a slight drop in free energy. For example, the change in free energy for CO_2 in 2W pyrophyllite (Figure 1d) transitioning from dimer state at $r = 4.1$ Å to individual molecules at $r = 12.0$ Å is approximately zero ($\Delta G_{r = 4.1 \rightarrow 12Å} = 0$) with ΔG^a= 0.29 kcal/mol. For comparison, in bulk water $\Delta G_{r = 3.0 \rightarrow 12Å} = -0.71$ kcal/mol. When further increasing nanoconfinement to 1W system, the dimeric form of CO_2 becomes the most favorable with $\Delta G_{r = 4.1 \rightarrow 12Å} = +0.65$ kcal/mol and $\Delta G^a = 0.73$ kcal/mol. Therefore, upon increasing the confinement, *e.g.*, from bulk water to 2W and 1W, the probability of CO_2 dimer formation increases significantly. A similar conclusion is reached for H_2 (Figure 1e). A head-to-head comparison between CO_2 and H_2 demonstrates that under hydrophobic pyrophyllite nanoconfinement (2W and 1W), CO_2 has a stronger tendency to form dimers because of robust quadrupole-quadrupole attraction. For instance, in the 1W system (green line), the $\Delta G_{r = 3.0 \rightarrow 12Å}$ for H_2 is +0.41 kcal/mol, which is about 40% smaller than that of CO_2. Furthermore, we still observe a decreasing trend in the PMF of H_2, compared to a rather flat tail of the CO_2 PMF prolife. This implies that the entropic contribution to H_2 PMF is still observable (probably because of the small size of H_2) in the 1W system.

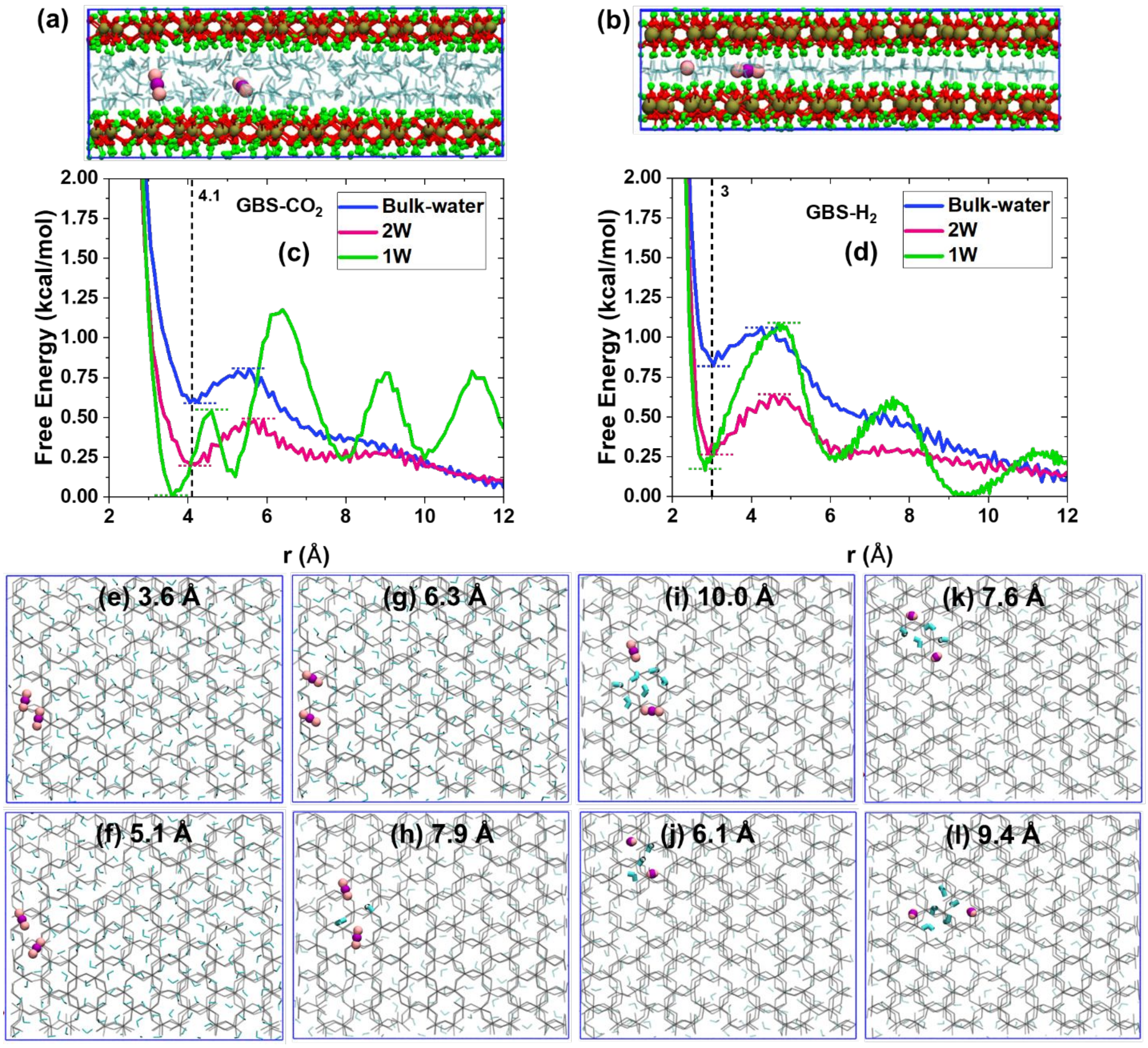

Figure 2. Simulation snapshots of two CO_2 or H_2 molecules in (a) 2W and (b) 1W gibbsite interlayers. See Figure 1 for color code. The simulation box dimensions perpendicular to the surface are 15.69 Å and 12.48 Å, respectively. The free energy profile as a function of distance r between two (c) CO_2 and (d) H_2 molecules confined within hydrated gibbsite (GBS) interlayer. (e), (f), (g), (h), and (i) are the simulation snapshots of CO_2 within 1W gibbsite interlayer at distance r of 3.6 Å, 5.1 Å, 6.3 Å, 7.9 Å, and 10.0 Å, respectively. (j), (k), and (l) are the simulation snapshots of H_2 within 1W gibbsite interlayer at distance r of 6.1 Å, 7.6 Å and 9.4 Å, respectively. Note, gibbsite surface is represented by grey color in snapshots e-l for the clarity and in a few snapshots, water molecules between two gas molecules are highlighted. The convergence of the PMF calculation is reported in SI, Figure S3.

To elucidate the influence of surface chemistry (hydrophobicity) on gas dimer formation, we calculate the PMF for two gases confined in 2W (Figure 2a) and 1W (Figure 2b) gibbsite systems. Overall, the PMF profiles for CO_2 (Figure 2c) and H_2 (Figure 2d) demonstrate that increasing hydrophilic nanoconfinement also increases the tendency of dimer formation, similar to the conclusion drawn for hydrophobic pyrophyllite system in Figure 1. Although the PMF profiles for CO_2 and H_2 in 2W gibbsite are comparable to 2W pyrophyllite, the PMF for 1W gibbsite exhibits unique characteristics (Figure 2c and 2d) due to the strongly structured water in 1W hydrophilic nanopore. In bulk water, hydrophobic 1W and 2W pyrophyllite, and 2W gibbsite systems, the PMF profile decreases smoothly as a function of *r* at larger distances. However, in 1W gibbsite, the PMF exhibits multiple minima and maxima for both H_2 and CO_2 as *r* increases.

At a smaller distances (e.g., $r < 6$ Å), gas-gas interactions and the relative orientation of CO_2 molecules[52] play a decisive role in the PMF profile. For example, at r = 3.6 Å (minimum on the PMF profile) in the 1W gibbsite system, the CO_2 dimer is in a "slipped parallel" arrangement (Figure 2e), which is one of the most energetically favored orientation in the gas phase.[52] At r = 5.1 Å, the dimer is in a "T" arrangement (Figure 2f) leading to a minimum energy at this position. At r = 6.3 Å, two CO_2 molecules are perfectly parallel (Figure 2g) resulting a strong $\mathrm{O}^{\delta-}_{\mathrm{CO_2}} - \mathrm{O}^{\delta-}_{\mathrm{CO_2}}$ and $\mathrm{C}^{2\delta+}_{\mathrm{CO_2}} - \mathrm{C}^{2\delta+}_{\mathrm{CO_2}}$ repulsions, possibly reflected in the global maximum. This maximum indicates that in an equilibrium simulation the probability of observing the parallel configuration is very low. One CO_2 molecule can easily rotate to form an energetically stable "T" arrangement (Figure 2f, i.e., energy minimum at 5.1Å), or two CO_2 molecules can be further separated to the minimum at 7.9 Å. At larger distances than 5.1 Å, the PMF is predominantly governed by the extent of hydrogen bonding between water-water and water-gibbsite. For CO_2 at the 7.9 Å minimum, there is only one layer of water molecules between two CO_2 molecules (Figure 2h), while at the 10 Å minimum there are two layers (Figure 2i). Transitioning from one minimum to another requires CO_2 molecules to overcome an energy barrier at 8.9 Å, requiring disruption of strong water-water and water-gibbsite interactions. For similar reasons, the PMF profile for H_2 displays multiple minima and maxima, where the transition from 9.5 Å minimum to 6.1 Å minimum, and vice versa, necessitates overcoming an energy barrier at 7.6 Å (Figure 2j, 2k, and 2l). Unlike CO_2, the gas orientation dependent PMF features are absent in H_2 due to extremely weak H_2-H_2 interaction. In addition, in the 1W gibbsite system, we also observe a decreasing trend for H_2 and not for CO_2 when r increases, similar to the observation in the 1W hydrophobic pyrophyllite system.

Note that the PMF profile is the result of a complex interplay of multiple interactions, including surface-water, water-water, water-gas, gas-gas, and gas-surface interactions, as well as an entropic effect. The computed free energy is the most comprehensive result to discuss the interaction of two gases in an environment. It is exceedingly complex to isolate and quantify the contribution of each component, making it challenging to pinpoint the precise cause of these observed features. Therefore, the previous discussion of the effect of structured water or arrangement of CO_2 on the observed maxima and minima is subjective, yet reasonable.

Our PMF results in Figures 1 and 2 predict that regardless of surface chemistry, increasing nanoconfinement increases the tendency for gas dimer and possibly gas cluster formation. To further support this conclusion and explore the possibility of forming a larger gas cluster than a dimer in nanopore, we perform representative simulations with 10 gas molecules within the 1W and 2W hydrated interlayers of pyrophyllite and gibbsite (see SI for details). Multiple realizations with different sizes of gas clusters are in dynamic equilibrium, as shown in Figure 3a-3c, for pyrophyllite 1W system. In Figure 3a, most gas molecules are spread homogeneously without forming a gas cluster. In Figure 3b, there is a large gas cluster along with individual gas molecules. In Figure 3c, almost all molecules are part of a cluster. To examine how different interlayer chemistry (pyrophyllite/gibbsite), different gases (CO_2/H_2), and different levels of confinement (1W/2W) favor one realization over others, we compute the weighted probability distribution (p_i^w) using the following equations:

$$p_i^w = \frac{s_i p_i}{\sum s_i p_i} \tag{1}$$

$$p_i = \frac{n_i}{\sum n_i} \tag{2}$$

Where, s_i is the size of cluster defined by number of gas molecules within a cut-off distance, n_i is the number of clusters, and p_i is the probability to find a cluster of a given size. The cut-off distance between two molecules is defined with respect to $\mathrm{C_{CO_2}} - \mathrm{C_{CO_2}}$ in CO_2 and $\mathrm{D_{H_2}} - \mathrm{D_{H_2}}$ in H_2 (description of labels is given in Figure 1) and is set to 4.1 Å and 3.0 Å, respectively. These cut-off distances correspond to the values at local minimum in the PMF profiles shown in Figure 1 and 2. Note that p_i is the probability of finding a cluster of size s_i, while p_i^w is the probability of finding a gas molecule in a cluster of size s_i. Calculating p_i^w is of significance here as we aim to determine the most favorable cluster size.

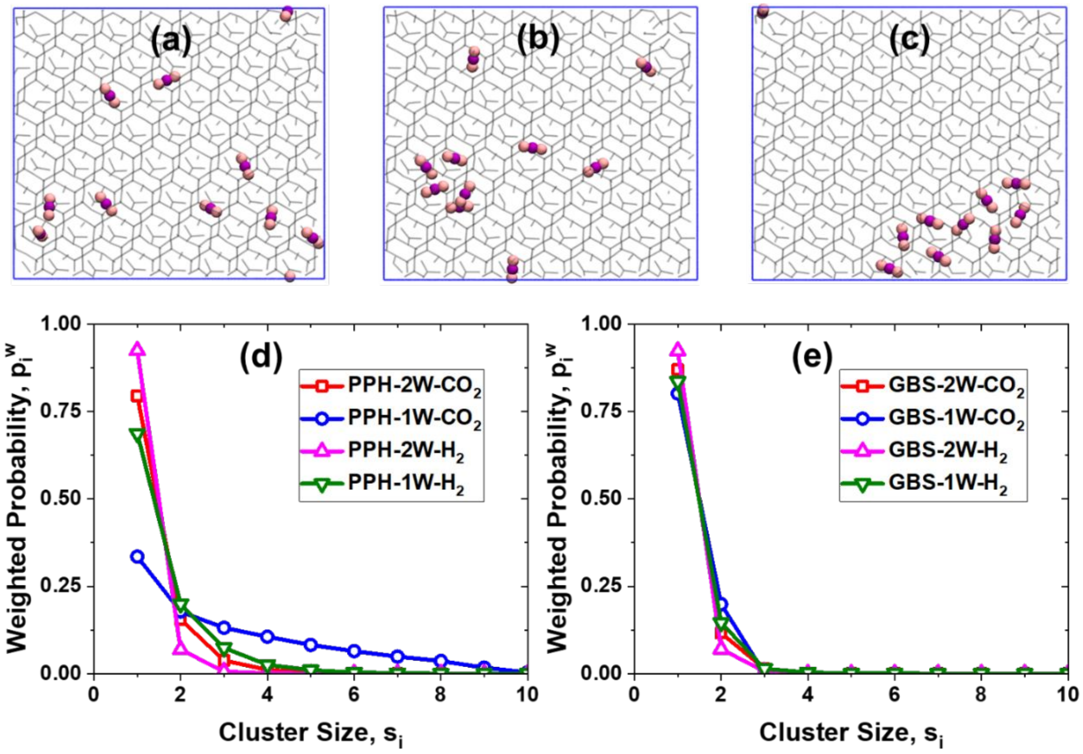

Figure 3. Simulation snapshots (a, b, c) showing different state of gas molecules in 1W hydrated pyrophyllite interlayer. Pyrophyllite is represented by grey color and water molecules are not shown for clarity. The weighted probability distribution (p_i^w) indicating the probability of finding a gas molecule in a given cluster size (s_i) within hydrated interlayer of (d) pyrophyllite (PPH) and (e) gibbsite (GBS). Details of simulations are reported in SI.

The p_i^w for CO_2 and H_2 within 2W and 1W hydrated pyrophyllite interlayer is given in Figure 3d. For CO_2, the p_i^w at $s_i = 1$ is higher for 2W than for 1W, suggesting a higher probability of CO_2 molecules to exist as individual molecule in 2W compared to 1W. However, at larger s_i, the p_i^w is higher for 1W than for 2W. For example, there is a possibility to observe a cluster of 8 CO_2 molecules in the 1W system but never in the 2W system. A similar behavior is evident for H_2, where the p_i^w at $s_i = 1$ is higher for 2W than for 1W, while it is opposite for $s_i \geq 2$. These observations for both CO_2 and H_2 confirm the enhancement of gas clustering in the 1W system compared to the 2W system. This phenomenon is consistent with the PMF results presented earlier, where we found that 1W provides a favorable environment for the formation of dimers compared to the 2W system. In addition, the lower p_i^w at $s_i = 1$ and higher p_i^w for $s_i \geq 2$ for CO_2 compared to those for H_2 confirm a stronger tendency for CO_2 to form larger clusters than H_2, which again supports the PMF profile presented in Figure 1.

Comparison of the results in Figure 3d for pyrophyllite and Figure 3e for gibbsite indicates a strikingly different behavior of gases in hydrophobic and hydrophilic nanopores. In gibbsite 2W and 1W systems (Figure 3e), for both CO_2 and H_2, the p_i^w for $s_i > 2$ is 0, indicating that the likelihood of finding a gas molecule in a large cluster is negligible. Instead, gases prefer to exist either as individual molecule or as dimers. The tendency to form a dimer is higher in 1W than in 2W systems, which is consistent with our PMF results in Figure 2 (i.e., nanoconfinement enhances dimer formation). To form a larger cluster than a dimer, gas molecules need to dehydrate a large region within a nanopore. With strong water-gibbsite interactions, this is impossible for gases to achieve. However, for weaker water-pyrophyllite interactions (Figure 3d), gas can dehydrate and form a larger cluster than a dimer.

The results presented so far demonstrate the effects of nanoconfinement and surface hydrophobicity on gas dimer and larger cluster formation. In the rest of this paper, we present the results to address the question: Does gas prefer to enter a nanopore (from bulk environment/macropore) as a dimer or as a single molecule? We compute the free energy landscape of individual gas molecule and gas dimer intercalating from vacuum to 2W pyrophyllite/gibbsite interlayers using the systems reported in Figure 4. The pyrophyllite and gibbsite structures in Figure 4a and 4b have edges that allow water and gas exchange between the interlayer and external environment. Note, the systems discussed in Figures 1, 2, and 3 have no edges and species (gas/water) were predefined in the interlayers. The free energy profiles of gas intercalation into 2W pyrophyllite and gibbsite interlayers are reported in Figure 4 c-f. The distance r in these plots is the distance of the center-of-mass of individual molecule or dimer from the vacuum phase along z-direction, where $r = 0$ corresponds to single/dimer molecules in vacuum phase while r beyond the dashed line (position of edge) denotes the location inside the nanopore (we just calculate the PMF for half of the pyrophyllite or gibbsite length). To create a dimer, the central atom (C_{CO_2} or D_{H_2}) of two gas molecules are artificially constrained by a harmonic spring with a force constant of 20 kcal/mol and an equilibrium distance of 4.1 and 3.0 Å (position of first local minima on the PMF profile in Figure 1) for CO_2 and H_2, respectively.

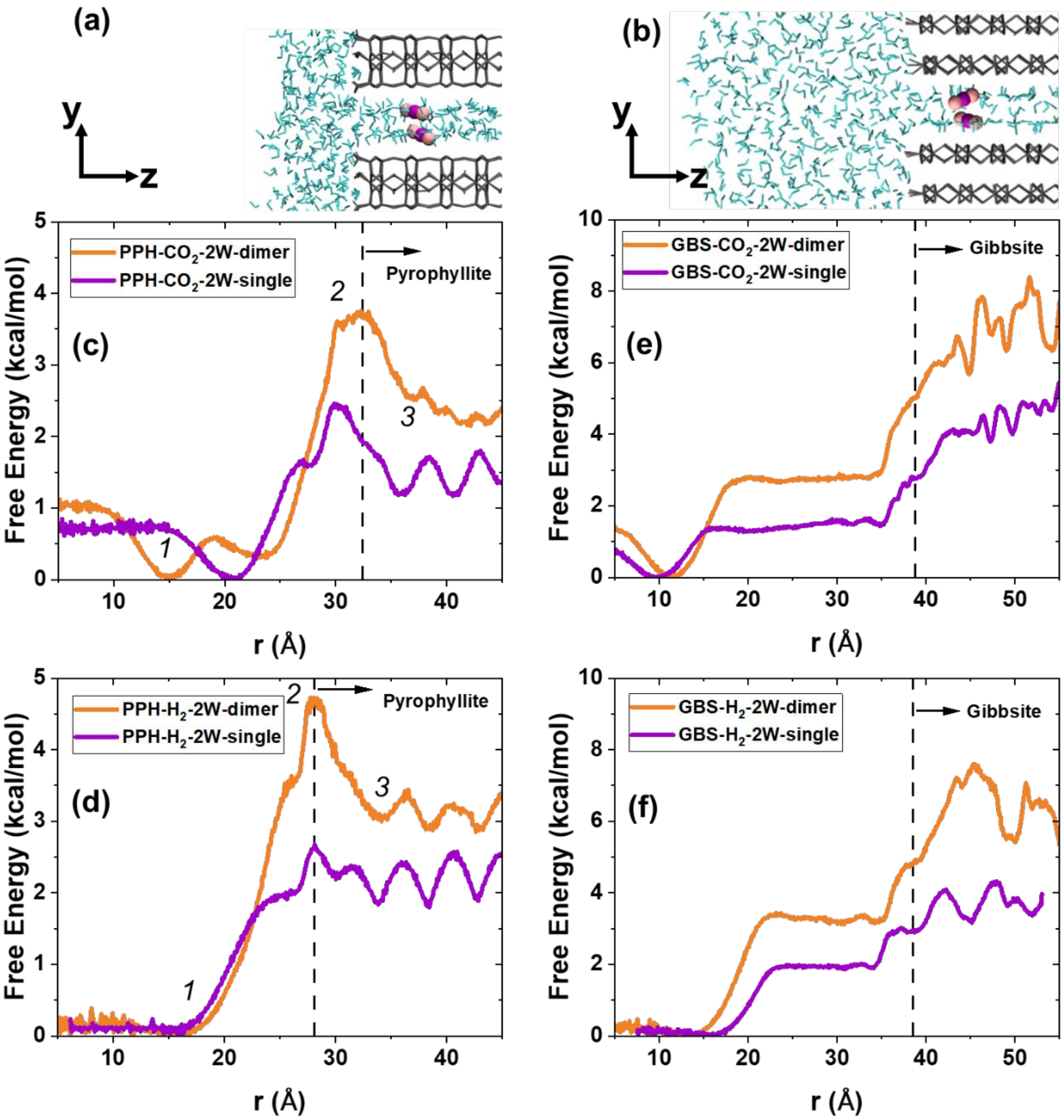

Figure 4. Snapshots displaying the simulation systems use to calculate the PMF of the intercalation of single/dimeric form of CO_2/H_2 molecules inside (a) pyrophyllite (PPH) and (b) gibbsite (GBS) interlayers. Pyrophyllite and gibbsite layers are represented by grey color. Note that these snapshots present just half of the system, a full simulation system is presented in Figure S6. The method to build the structure with edges can be found in the SI. The free energy profiles of (c) CO_2 and (d) H_2 molecules moving from vacuum to 2W hydrated pyrophyllite interlayer. The free energy profiles of (e) CO_2 and (f) H_2 molecules intercalating from vacuum to 2W hydrated gibbsite interlayer. Simulation setups and the convergence of the PMF calculation is reported in SI (Figure S7 and Figure S8).

The PMF profile in Figure 4c indicates that individual CO_2 molecule or CO_2 dimer prefer to accumulate at the vacuum/water interface (minimum at position 1 in Figure 4c and also Figure S6a). To enter the nanopore, the CO_2 molecule/dimer needs to overcome an energy barrier at position 2, i.e., the pore opening (Figure S6b). The energy barrier at the pore opening arises from the disruption of strong hydrogen bond between –OH groups present at the pyrophyllite edge and water molecules. The CO_2 dimer experiences a much higher barrier than the individual CO_2 molecule. This implies that the intercalation of individual molecule is faster than that of dimer. The change in free energy ($\Delta G_{vacuum \rightarrow interlayer}$) when going from vacuum to the hydrated interlayer is slightly positive (< 0.5 kcal/mol) for single molecule (e.g., at position 3, Figure S6c), while it is largely positive (> 1 kcal/mol) for dimer. This indicates that intercalation of a single molecule into pyrophyllite nanopores is favored over CO_2 dimer. We want to emphasize that a CO_2 dimer is not likely to enter the pore as a pair, but a CO_2 dimer can be formed inside the pore when two individual CO_2 molecules are present. Following intercalation, we observe a series of local minima and maxima in a wave-like pattern for a single molecule. The local minima denote the positions of CO_2 in the siloxane rings and local maxima are observed when the CO_2 molecule locates on top of siloxane rim while transitioning from one ring to another, as discussed in our previous work on the CO_2 intercalation into montmorillonite interlayer.[4] This wave-like feature is absent for dimer as its size is too large to reflect the molecular details of the surface.

Interestingly, during CO_2 deintercalation from the pyrophyllite interlayer to the vacuum, the ΔG^a for both the dimer and single molecule is comparable. Whereas, $\Delta G_{interlayer \rightarrow vacuum}$ is more negative for the dimer than a single molecule. This indicates that the deintercalation is favored when the gas exists in the form of a cluster. Thus, CO_2 molecules preferentially intercalate inside the hydrated pyrophyllite nanopore as individual/single molecule, and then aggregate to form dimers or larger clusters. If released from the nanopore, CO_2 molecules preferentially exit as dimers/clusters. This discussion agrees with previous work,[3] even though in this work CO_2 molecules form clusters in water, while in previous work CO_2 molecules form clusters in a gas phase.

The free energy landscapes for the intercalation of single and dimeric forms of H_2 (Figure 4d) confirm that the intercalation of a H_2 (in any form) inside the pyrophyllite nanopores is unfavorable, and the H_2 dimer experiences a higher energy barrier and a higher free energy for the transition. Compared to CO_2, the $\Delta G_{vacuum \rightarrow interlayer}$ for H_2 is higher. These findings agree with our previous conclusion that low solubility of H_2 in hydrated clay interlayers limits gas loss in hydrogen geological storage.[16]

For hydrophilic gibbsite 2W interlayer (Figure 4b), the $\Delta G_{vacuum \rightarrow nanopore}$ and ΔG^a is notably higher for dimers than single CO_2 (Figure 4e) or H_2 (Figure 4f) molecules, demonstrating extreme difficulty for a single gas molecule or dimer to intercalate into the nanopore. This difficulty arises from strong gibbsite-water interaction inside the hydrated interlayer. As a consequence, gas intercalation results in a disruption of hydrogen bond networks and unfavorable rearrangement of the water molecules.

3. Conclusions

In conclusion, we employed metadynamic molecular simulations to investigate H_2 and CO_2 dimer/cluster formation within the water-saturated nanopores. Two distinct nanopore environments, characterized as hydrophobic (pyrophyllite) and hydrophilic (gibbsite) were explored. The results highlighted the substantial influence of hydrophobic and hydrophilic nanoconfinement on gas cluster formation. Within the hydrophobic nanopore, CO_2 exhibited a stronger tendency for cluster formation than H_2, attributable to quadrupole-quadrupole attraction. Conversely, within the hydrophilic nanopore, robust hydrogen bonding between water and the gibbsite surface suppresses cluster formation. Intriguingly, irrespective of surface chemistry, increasing the extent of confinement favors dimer formation. We also assessed the free energy associated with the intercalation of singular and dimeric forms of these gases from vacuum to a hydrated nanopore. The results indicate that gas prefers to enter the nanopores as an individual molecules but escape the nanopores as a dimer or cluster. This comprehensive study has developed fundamental insights into cluster formation under nanoconfinement and delved into the broader implications of these findings on the geological storage of H_2 and CO_2.

Author contributions

A.C. contributed to investigation, formal analysis, methodology, and writing – original draft; T.H contributed to writing – review & editing, and supervision.

Conflicts of interest

There are no conflicts to declare.

Acknowledgements

This article has been authored by an employee of National Technology & Engineering Solutions of Sandia, LLC under Contract No. DE-NA0003525 with the U.S. Department of Energy (DOE). The employee owns all right, title and interest in and to the article and is solely responsible for its contents. The United States Government retains and the publisher, by accepting the article for publication, acknowledges that the United States Government retains a non-exclusive, paid-up, irrevocable, world-wide license to publish or reproduce the published form of this article or allow others to do so, for United States Government purposes. The DOE will provide public access to these results of federally sponsored research in accordance with the DOE Public Access Plan https://www.energy.gov/downloads/doe-public-access-plan. This work was supported by a Laboratory Directed Research & Development (LDRD) project. We would like to thank you Prof. Ward Thompson at University of Kansas for useful discussion.

References

1. J. Rabinowitz, E. Whittier, Z. Liu, K. Jayant, J. Frank and K. Shepard, *Science Advances*, 2020, **6**, eabd0126.
2. A. Agarwal, W. J. Ng and Y. Liu, *Chemosphere*, 2011, **84**, 1175-1180.
3. M. Tsotsalas, P. Hejcik, K. Sumida, Z. Kalay, S. Furukawa and S. Kitagawa, *Journal of the American Chemical Society*, 2013, **135**, 4608-4611.
4. T. A. Ho, Y. Wang, S. B. Rempe, N. Dasgupta, C. T. Johnston, G. Xu, T. S. Zwier and M. Mills, *The Journal of Physical Chemistry Letters*, 2023, **14**, 2901-2909.
5. M. Fan, D. Tao, R. Honaker and Z. Luo, *Mining Science and Technology (China)*, 2010, **20**, 159-177.
6. Y. Wang, X. Li, Y. Zhou, P. Huang and Y. Xu, *International Journal of Pharmaceutics*, 2010, **384**, 148-153.
7. R. M. M. Smeets, U. F. Keyser, M. Y. Wu, N. H. Dekker and C. Dekker, *Physical Review Letters*, 2006, **97**, 088101.
8. M. R. Powell, L. Cleary, M. Davenport, K. J. Shea and Z. S. Siwy, *Nature Nanotechnology*, 2011, **6**, 798-802.
9. X. H. Zhang, X. Zhang, J. Sun, Z. Zhang, G. Li, H. Fang, X. Xiao, X. Zeng and J. Hu, *Langmuir*, 2007, **23**, 1778-1783.
10. J. W. G. Tyrrell and P. Attard, *Physical Review Letters*, 2001, **87**, 176104.
11. N. Ishida, T. Inoue, M. Miyahara and K. Higashitani, *Langmuir*, 2000, **16**, 6377-6380.
12. T. A. Ho, Y. Wang, A. Ilgen, L. J. Criscenti and C. M. Tenney, *Nanoscale*, 2018, **10**, 19957-19963.
13. Y. Wang and B. Bhushan, *Soft Matter*, 2010, **6**, 29-66.
14. J. L. Parker, P. M. Claesson and P. Attard, *The Journal of Physical Chemistry*, 1994, **98**, 8468-8480.
15. A. Agrawal, J. Park, D. Y. Ryu, P. T. Hammond, T. P. Russell and G. H. McKinley, *Nano Letters*, 2005, **5**, 1751-1756.
16. T. A. Ho, C. F. Jove-Colon and Y. Wang, *Sustainable Energy & Fuels*, 2023, **7**, 3232-3238.
17. C. Li, Z. Zhang and L. Heinke, *Physical Chemistry Chemical Physics*, 2022, **24**, 3994-4001.
18. D. S. Sholl and K. A. Fichthorn, *Physical Review Letters*, 1997, **79**, 3569-3572.
19. B. Coasne and D. Farrusseng, *Microporous and Mesoporous Materials*, 2019, **288**, 109561.
20. A. Phan, D. R. Cole and A. Striolo, *The Journal of Physical Chemistry C*, 2014, **118**, 4860-4868.
21. C.-C. Liu, H.-J. Chou, C.-Y. Lin, D. Janmanchi, P.-W. Chung, C.-Y. Mou, S. S. F. Yu and S. I. Chan, *Microporous and Mesoporous Materials*, 2020, **293**, 109793.
22. L. N. Ho, S. Clauzier, Y. Schuurman, D. Farrusseng and B. Coasne, *The Journal of Physical Chemistry Letters*, 2013, **4**, 2274-2278.
23. L. N. Ho, Y. Schuurman, D. Farrusseng and B. Coasne, *The Journal of Physical Chemistry C*, 2015, **119**, 21547-21554.
24. B. Dong, Y. Pei, N. Mansour, X. Lu, K. Yang, W. Huang and N. Fang, *Nature Communications*, 2019, **10**, 4815.
25. S. B. Mishra, A. Choudhary, S. C. Roy and B. R. K. Nanda, *Physical Review Materials*, 2018, **2**, 115801.
26. S. Baek and I. Y. Akkutlu, *SPE Journal*, 2021, **26**, 2018-2037.
27. J. N. Israelachvili, *Intermolecular and surface forces*, Academic press, 2011.
28. A. W. Knight, N. G. Kalugin, E. Coker and A. G. Ilgen, *Scientific Reports*, 2019, **9**, 8246.
29. F. Leoni, C. Calero and G. Franzese, *ACS Nano*, 2021, **15**, 19864-19876.
30. W. Sparreboom, A. van den Berg and J. C. T. Eijkel, *Nature Nanotechnology*, 2009, **4**, 713-720.
31. J. A. Greathouse, T. J. Duncan, A. G. Ilgen, J. A. Harvey, L. J. Criscenti and A. W. Knight, *Environmental Science: Nano*, 2021, **8**, 1992-2005.

32. G. Algara-Siller, O. Lehtinen, F. C. Wang, R. R. Nair, U. Kaiser, H. A. Wu, A. K. Geim and I. V. Grigorieva, *Nature*, 2015, **519**, 443-445.
33. S. Ruiz-Barragan, D. Muñoz-Santiburcio, S. Körning and D. Marx, *Physical Chemistry Chemical Physics*, 2020, **22**, 10833-10837.
34. F. Deißenbeck, C. Freysoldt, M. Todorova, J. Neugebauer and S. Wippermann, *Physical Review Letters*, 2021, **126**, 136803.
35. K. Leung, *Nano Letters*, 2023, **23**, 8868-8874.
36. E. Chiavazzo, M. Fasano, P. Asinari and P. Decuzzi, *Nature Communications*, 2014, **5**, 3565.
37. J. A. Delgado, V. I. Águeda, M. A. Uguina, J. L. Sotelo, P. Brea and C. A. Grande, *Ind Eng Chem Res*, 2014, **53**, 15414-15426.
38. A. Barducci, G. Bussi and M. Parrinello, *Phys Rev Lett*, 2008, **100**, 020603.
39. T. A. Ho and Y. Wang, *ACS Applied Materials & Interfaces*, 2021, **13**, 41330-41338.
40. S. Plimpton, *Journal of Computational Physics*, 1995, **117**, 1-19.
41. D. J. Evans and B. L. Holian, *The Journal of Chemical Physics*, 1985, **83**, 4069-4074.
42. W. G. Hoover, *Physical Review A*, 1985, **31**, 1695-1697.
43. R. T. Cygan, J.-J. Liang and A. G. Kalinichev, *The Journal of Physical Chemistry B*, 2004, **108**, 1255-1266.
44. H. J. C. Berendsen, J. R. Grigera and T. P. Straatsma, *The Journal of Physical Chemistry*, 1987, **91**, 6269-6271.
45. J. J. Potoff and J. I. Siepmann, *AIChE Journal*, 2001, **47**, 1676-1682.
46. C. Lopez-Lazaro, P. Bachaud, I. Moretti and N. Ferrando, *Bulletin de la Société Géologique de France*, 2019, **190**.
47. O. A. Moultos, I. N. Tsimpanogiannis, A. Z. Panagiotopoulos and I. G. Economou, *The Journal of Physical Chemistry B*, 2014, **118**, 5532-5541.
48. T. A. Ho, S. T. Dang, N. Dasgupta, A. Choudhary, C. S. Rai and Y. Wang, *International Journal of Hydrogen Energy*, 2024, **51**, 158-166.
49. M. W. Mahoney and W. L. Jorgensen, *The Journal of Chemical Physics*, 2001, **115**, 10758-10768.
50. M. Ceriotti, W. Fang, P. G. Kusalik, R. H. McKenzie, A. Michaelides, M. A. Morales and T. E. Markland, *Chemical Reviews*, 2016, **116**, 7529-7550.
51. M. Ceriotti, J. Cuny, M. Parrinello and D. E. Manolopoulos, *Proceedings of the National Academy of Sciences*, 2013, **110**, 15591-15596.
52. M. Saharay and S. Balasubramanian, *The Journal of Physical Chemistry B*, 2007, **111**, 387-392.